AGU PUBLICATIONS

Water Resources Research

RESEARCH ARTICLE
10.1002/2017WR020561

Key Points:
- Field observations, LiDAR data, and historical information are combined to investigate meander dynamics
- Vegetation dynamics are strongly related to scroll, ridge, and swale evolution on inner banks
- Results can inform modeling aimed at describing floodplain formation in meandering rivers

Correspondence to:
S. Zen,
simone.zen@unitn.it

Citation:
Zen, S., A. M. Gurnell, G. Zolezzi, and N. Surian (2017), Exploring the role of trees in the evolution of meander bends: The Tagliamento River, Italy, *Water Resour. Res.*, *53*, 5943–5962, doi:10.1002/2017WR020561.

Received 10 FEB 2017
Accepted 22 JUN 2017
Accepted article online 5 JUL 2017
Published online 24 JUL 2017

Exploring the role of trees in the evolution of meander bends: The Tagliamento River, Italy

Simone Zen[1], Angela M. Gurnell[2], Guido Zolezzi[1], and Nicola Surian[3]

[1]Department of Civil, Environmental and Mechanical Engineering, University of Trento, Italy, [2]School of Geography, Queen Mary University of London, London, UK, [3]Department of Geosciences, University of Padua, Padua, Italy

Abstract To date, the role of riparian trees in the formation of scroll bars, ridges, and swales during the evolution of meandering channels has been inferred largely from field observations with support from air photographs. In situ field observations are usually limited to relatively short periods of time, whereas the evolution of these morphological features may take decades. By combining field observations of inner bank morphology and overlying riparian woodland structure with a detailed historical analysis of airborne LiDAR data, panchromatic, and color images, we reconstruct the spatial and temporal evolution of the morphology and vegetation across four meander bends of the Tagliamento River, Italy. Specifically we reveal (i) the appearance of deposited trees and elongated vegetated patches on the inner bank of meander bends following flood events; (ii) temporal progression from deposited trees, through small to larger elongated vegetated patches (pioneer islands), to their coalescence into long, linear vegetated features that eventually become absorbed into the continuous vegetation cover of the riparian forest; and (iii) a spatial correspondence between the resulting scrolls and ridge and swale topography, and tree cover development and persistence. We provide a conceptual model of the mechanisms by which vegetation can contribute to the formation of sequence of ridges and swales on the convex bank of meander bends. We discuss how these insights into the biomorphological processes that control meander bends advance can inform modeling activities that aim to describe the lateral and vertical accretion of the floodplain during the evolution of vegetated river meanders.

1. Introduction

As meander bends evolve and migrate laterally, scroll bars often form along the inner bank across the surface of point bars [*Hickin*, 1974]. The scrolls are then incorporated into the floodplain as the river migrates and are often preserved as a series of ridges and swales that corrugate the floodplain surface.

The mechanisms leading to scroll formation have attracted interest since at least the 1950s [e.g., *Sundborg*, 1956]. Many contributory and not necessarily mutually exclusive formative physical processes have been suggested [*Nanson and Croke*, 1992] including the following:

i. The migration of transverse bars from the channel of sand bed rivers onto the point bar [*Sundborg*, 1956; *Jackson*, 1976; *Kleinhans and van den Berg*, 2011].
ii. Sediment deposition against the convex bank associated with zones of flow separation [*Bagnold*, 1960; *Leeder and Bridges*, 1975; *Blanckaert et al*., 2013; *Kasvi et al*., 2013].
iii. The formation of an initial coarse sediment point bar platform on which, in rivers with a bimodal size range of bed load, a scroll bar of finer material develops [*Nanson*, 1980, 1981].
iv. The formation of a chute channel between the convex bank and point bar on coarse grained point bars [*McGowan and Garder*, 1970; *Grenfell et al*., 2012].
v. Inner-bank deposition following rapid cutbank erosion that leads to channel widening [*Nanson*, 1981; *Kleinhans and van den Berg*, 2011]. This process is supported by recent laboratory experiments in which channel widening, caused by bank retreat near the bend apex, has been observed to cause deposition of scroll ridges [*van de Lageweg et al*., 2015].

The recurrence interval of conditions for the initiation of a scroll bar appears to vary widely, with an average recurrence interval of approximately 30 years observed within a section of the Beatton River, British Columbia [*Nanson*, 1980], and recurrence intervals of decades to centuries suggested by *Bridge et al*. [1995].

Furthermore, once formed ridges and swales can persist on floodplains, even where overbank sediment deposition is substantial, because the floodplain ridges are maintained by secondary currents which move sediment from the swales towards the ridge crests [*Nanson*, 1980; *Nanson and Croke*, 1992].

Environmental conditions in the scroll or ridge and swale zones are sufficiently different to support distinct plant communities [e.g., *Hickin*, 1974; *Salo et al*., 1986; *Colonnello*, 1990], and vegetation has often been mentioned as being a supporting factor in scroll and ridge and swale development. For example, in association with process (i) [*Nanson and Croke*, 1992] and process (iii) [*Nanson*, 1980; *Rozo et al*., 2012], establishment of floodplain vegetation on the ridge crests can enhance scroll development and transformation into a floodplain ridge. Indeed, *Hupp* [2000] noted that on the floodplains of the south-eastern United States, "nearly imperceptible changes in elevation may result in distinct pervasive changes in species composition and zonation, strongly suggesting a rigorous relationship between vegetation and hydrogeomorphological processes" [*Hupp*, 2000, p. 3008].

Some researchers have gone further in highlighting both dead and living vegetation as significant causal factors in scroll formation and development. On the Beatton River, *Nanson and Beach* [1977] observed that deposition on bars induced by sprouting poplar trees buried the surface on which the plants had established by about 2.5 m, resulting in vertical and lateral aggradation of the bars. *Nanson* [1981] also observed on the same river that large pieces of dead wood, including entire uprooted trees, became stranded and buried during the wide-channel phase of mechanism (v), altering flow patterns across point bar surfaces and so leading to the development and extension of a linear ridge on the point bar [*Nanson*, 1981]. *Hickin* [1984] proposed an extension to this process by observing that rafts of forest litter, mosses, and young tree seedlings may also become grounded on point bars leading to vegetation establishment and an enhanced rate of sedimentation. Observations of ridge (i.e., scroll) development on bars by *McKenney et al*. [1995] illustrated the potential importance of tree seed deposition in their formation. *McKenney et al*. [1995] described a model for the interaction between channel morphogenesis and vegetation bands including five stages of linear ridge formation. First a bar with a bare gravel surface is (re)formed during a major flood. Second, seeds are deposited in a band parallel to the channel during a subsequent, smaller flood. Third, if sufficient moisture is available, the seeds germinate, and if ensuing flows do not disturb the seedlings, they grow. Fourth, during subsequent inundating floods, sediment is deposited in the developing vegetation bands because their flow resistance is higher than in the surrounding channel and chute. Fifth, flows become concentrated away from the aggrading vegetated bands leading to local deepening of the unvegetated areas and the development of vegetated linear ridges. This model and its incorporation of a linear band of germinating seeds is closely coupled to the "recruitment box" model for riparian cottonwood (Salicaceae) species [*Mahoney and Rood*, 1998].

Field observations, such as those described above, provide important information about the morphology and sedimentary structure of fluvial features and their potential association with vegetation colonization and development, but their interpretation is usually constrained by limitations in the time period spanned by such observations, even when supported by air photographs. As a result, understanding of the morphological development of features that may take several decades to develop can frequently only be inferred.

Remotely sensed data offer enormous potential to extend the time period of observations of land form development and its spatial coverage [e.g., *Fonstad and Marcus*, 2010; *Carbonneau and Piégay*, 2012] with the acquisition of hyperscale information increasingly generating data at a quality that can be comparable to direct field measurements [e.g., *Carbonneau et al*., 2012, *Williams et al*., 2014], providing the potential to quantify spatial patterns and temporal changes in many hydromorphological characteristics at very high resolution from reach to basin scales [e.g., *Bizzi et al*., 2016].

At the reach-scale, data sets acquired using satellite and airborne platforms provide an enormous range of information on the morphology and vegetation cover of the land surface. While aerial photography usually provides the longest temporal record [*Grabowski et al*., 2014], other data sets provide complementary information that permit a much deeper analysis. This has allowed many advances in the identification of vegetation form and dynamics that are relevant to fluvial landform evolution. For example, *Valente et al*. [2013] combine time series of the NDVI index extracted from MODIS-VI and Landsat ETM data with hydrological records and field observations to provide a better understanding of the relationships between vegetation, hydrological, and geomorphological patterns over an extensive area of the Middle Araguaia River, Brazil. At

a much finer spatial scale, *Antonarakis et al*. [2008], investigating meanders of the Garonne and Allier Rivers, France, illustrate how analysis of airborne LiDAR data not only allows the generation of detailed terrain maps but also supports detailed classification of land cover (water, bare sediment, and vegetation) and vegetation structure (young to mature riparian forest vegetation and plantation woodland). More recently, *Dufour et al*. [2013] explored the use of data sets obtained from several sources including LiDAR and radar, to monitor very detailed changes in the 3-D structure of riparian vegetation at a high spatial and temporal resolution. Of particular relevance to the present research is the work of *Rozo et al*. [2012], who undertook a temporal analysis of Landsat images combined with field measurements to investigate floodplain features of a part of an evolving anastomosing system of the middle Amazon River where meandering secondary channels show active scroll bar development.

Since the quantity and nature of the data sets available for any particular study site are highly variable, the challenge is to integrate information across time from different sources that may vary widely in their information content as well as their spatial resolution [*Grabowski and Gurnell*, 2016].

In this paper, we employ such an integrated approach to extend understanding of the role of trees in meander bend accretion. Specifically, with reference to the lower Tagliamento River, north-east Italy (Figure 1) we aim (i) to quantify the role of trees in the development of ridge-swale topography in the advancing inner

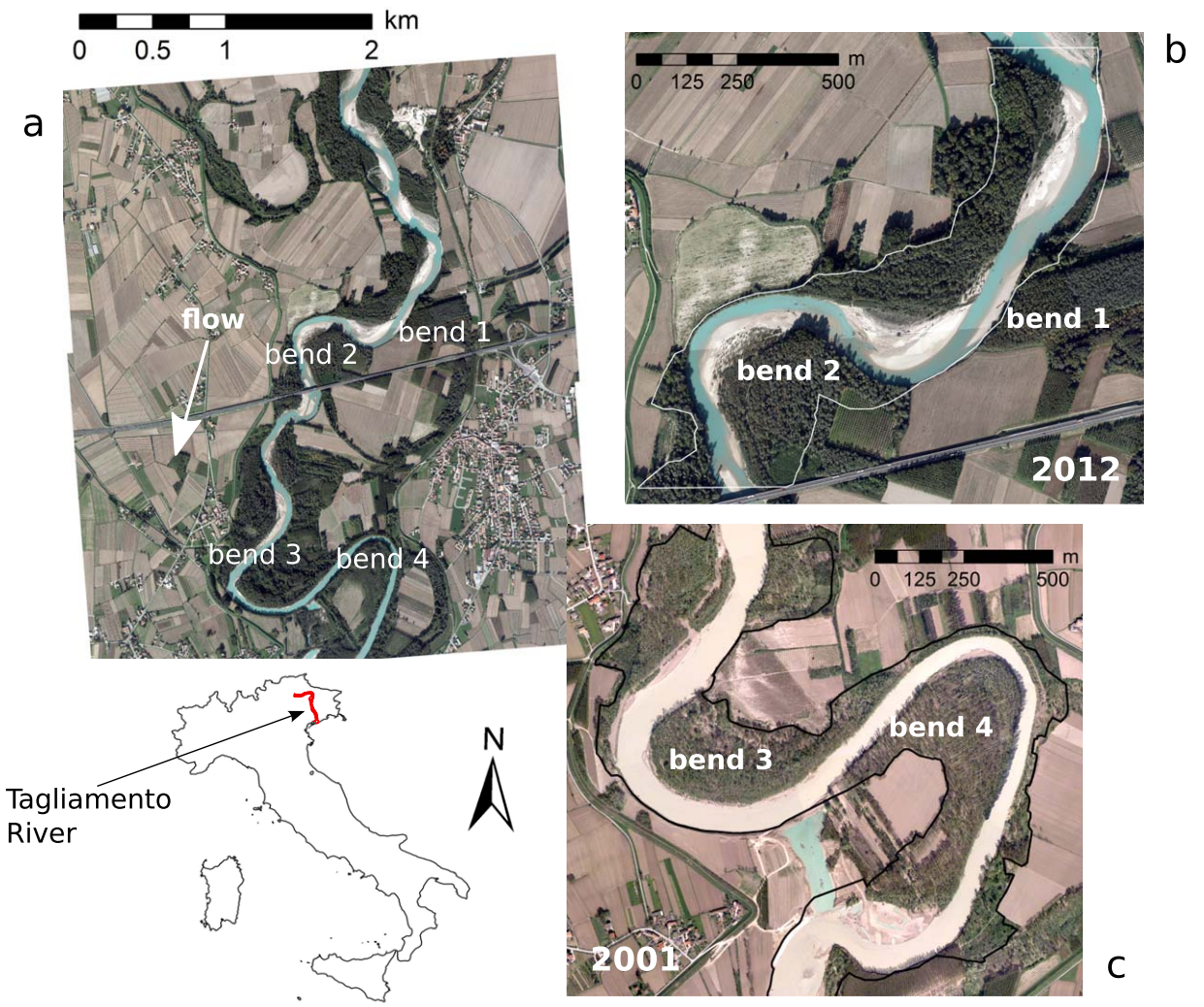

Figure 1. The study area, (a) the lower reaches of the Tagliamento River showing the locations of bends 1–4 in 2012—from 45°49′19″N, 12°59′19″E to 45°47′36″N, 12°58′42″E; (b) bends 1 and 2 in 2012; (c) bends 3 and 4 in 2001. The continuous lines shown in white in Figure 1b and black in Figure 1c indicate the portion of the riparian corridor that evolved naturally across the dates considered.

bank of meander bends and (ii) to detect the association between the coevolving floodplain topography and riparian vegetation that sustains the accretion process. We pursue these goals by combining an historical analysis of airborne imagery and LiDAR data with contemporary field measurements.

2. The Study Area

The research was conducted in the lower reaches of the gravel bed Tagliamento River, located in north east Italy. The river drains an area of 2580 km^2 from the Julian and Carnian Alps to the Adriatic Sea and has a flow regime typical of Alpine watersheds, whereby the contribution of both snowmelt and rainfall promotes high discharge variability throughout the year, with the highest flows occurring in spring and autumn. Low human pressures along the river have allowed a relatively natural riparian zone to be retained along most of the main stem. The river also displays different planform styles along its length. Braided and island braided patterns persist throughout most of the river's length with a transitional and then meandering planform in the lower reaches [*Gurnell et al*., 2000]. High variability in discharge and a high sediment load delivered to the lower reaches promote significant meander dynamics [*Surian et al*., 2009].

The present research was conducted within the meandering section of the Tagliamento River between 45°49′19″N, 12°59′19″E to 45°47′36″N, 12°58′42″E and focuses on four meander bends (1–4, Figure 1). Within the study area, the riparian woodland is dominated by *Populus nigra* [*Karrenberg et al*., 2003]. This species regenerates freely from uprooted trees and pieces of large wood deposited on moist, open areas of exposed sediments. This regeneration process is an important driver of vegetation colonization of bars along the Tagliamento River [*Gurnell et al*., 2001; *Gurnell and Petts*, 2006].

Although the Tagliamento River is one of the few large rivers within Europe that retain a relatively naturally functioning fluvial corridor, human activities within its lower reaches have encroached into the riparian woodland. In particular, woodland has been cleared for agriculture, including planting of commercial poplars. Furthermore, several constraints now affect the natural evolution of many of the river's meanders, including the installation of groynes and rip-rap, which have been introduced to prevent river bank erosion, preserve the cultivated areas, and stop the river reaching set-back flood levées [*Ziliani and Surian*, 2012]. Because of these factors, the present study was confined to four meander bends that are still bordered by naturally colonized riparian woodland (Figures 1b and 1c). Nevertheless, erosion control structures have been installed on the outer banks, preventing bends 3 and 4 (Figure 1c) from migrating freely for more than a decade and bend 2 (Figure 1b) since 2006. Therefore, the present analysis concentrates mainly on bend 1 and on bend 2 prior to 2006 (Figure 1b) but also refers to the meanders downstream (bends 3 and 4; Figure 1c) which show more complex morphological patterns and thus can support and extend findings from the analysis conducted on bends 1 and 2.

3. Methods

Three main data sources were used to investigate the morphology and riparian vegetation dynamics of the studied meander bends: airborne LiDAR, aerial images, and field measurements.

In order to compare results obtained from the analysis of data from these three sources, all data sets were registered to a common geographical base, the Gauss-Boaga Est datum Roma 1940 projection. In addition, all analyzed data sets were confined to the area enclosed by naturally colonized riparian vegetation. This area was defined by first digitizing its limits for each set of aerial images, and then overlaying these date-specific polygons to define a polygon which enclosed naturally colonized vegetation in all of the studied images (the white and black borders in Figures 1b and c, respectively).

3.1. Airborne LiDAR Data

LiDAR data were available from a survey conducted in April 2001. Analysis of this data set provided concurrent information on land surface morphology and vegetation cover.

The LiDAR data set was analyzed using FUSION software, which uses a hierarchical filtering algorithm [*Kraus and Pfeifer*, 1998] to filter the data and construct a Digital Elevation Model (DEM) of the ground surface. In doing so, it classifies the LiDAR points into terrain and vegetation, with the latter associated with points that protrude above the surrounding point cloud. This filter technique has been found to be most effective in

areas of subdued ground topography where the vegetation is sufficiently sparse for at least 25% of the returns to reach the ground surface [*Hollaus et al*., 2006]. A decrease in penetration depth associated with a more extensive vegetation cover, influences the accuracy of both DEM and canopy structure estimation [*Wasser et al*., 2013]. Both of the required conditions of subdued topography and sparse vegetation cover apply for the study area given the relatively flat floodplain location (but see below) and the early April survey date, when foliage was largely absent from the deciduous trees of the riparian forest.

To construct the DEM, the filtered ground surface points were resampled to a regular 2 m grid, by assigning the average value of the returns within each cell. A 2 m $\times$ 2 m spatial resolution was chosen as a compromise between detailed spatial definition of the DEM and a sufficient number of points within each cell, given that the filtered bare-ground data had an average return density of 0.78 m^{-2}. Unlike previous analyses of the middle reaches of the Tagliamento [*Bertoldi et al*., 2011], the relatively short length of the study reach and its low longitudinal slope (0.001) precluded the need to subtract the reach slope from the DEM before comparing morphological characteristics of subreaches. LiDAR does not penetrate the water surface and the homogenous color of the water in the air photographs associated with the 2001 survey prevented the use of optical techniques to reconstruct the bathymetry of the inundated area [*Bertoldi et al*., 2011]. Therefore, interpretation of the topographic data was confined to elevations above 4 m, to exclude analysis of all points that correspond to the water surface.

Vegetation height was estimated as the difference between the interpolated ground surface (DEM) and the raw LiDAR elevations. These data were processed in two ways. First, because of their low density (average horizontal distance between returns was 0.46 m), the point estimates of vegetation height were organized into a 6 m regular grid for further analysis of vegetation properties. The Canopy Height Model (CHM) was estimated from the maximum height of points that projected more than 1.5 m above the estimated ground surface within each 6 m $\times$ 6 m cell in order to avoid noise from returns close to the ground. Second, the presence of quite steep and high river banks in some locations required an additional filter operation to avoid classifying ground points that were close to the channel's steep banks as vegetation. A new ground surface was estimated which excluded the areas of the DEM showing local slopes greater than a 20° threshold, which was identified as the minimum value for the presence of distinct, high river banks. Using these procedures information on the maximum vegetation height was extracted for each grid cell.

3.2. Aerial and Satellite Images

Aerial and satellite images captured during thirteen different years between 1966 and 2015 (Table 1) were assembled to support investigation of riparian vegetation dynamics and their association with the evolution of the four meander bends (Figure 1). Images from 1983 to 2015 captured significant morphological changes within bends 1 and 2 (Figure 1b), whereas significant lateral migration of bends 3 and 4 (Figure 1c) was captured in images from 1966 to 2001. Later images were excluded because lateral channel adjustment at these bends was prevented by engineering works.

All images were visually inspected to identify evidence of the potential impact of vegetation colonization and growth on meander evolution, particularly scroll bar development.

Table 1. Details of the Images Analyzed in This Study[a]

Year (Date)	Type	Scale	Resolution (dpi)	Pixel Size (m)	Source
1966 (November–December)	B/W	1:12,490	800	0.40	Autorita di Bacino dei fiumi dell'Alto Adriatico
1970	B/W	1:13,310	800	0.41	Regione Friuli-Venezia Giulia
1983	B/W	1:18,050	800	0.55	Autorita di Bacino dei fiumi dell'Alto Adriatico
1993 (May–June)	B/W	1:31,810	1200	0.80	Autorita di Bacino dei fiumi dell'Alto Adriatico
1997 (June)	C	1:28,120	800	0.60	Autorita di Bacino dei fiumi dell'Alto Adriatico
2001 (April)	O,C			0.50	Autorita di Bacino dei fiumi dell'Alto Adriatico
2003 (27 September)	GE,C			1.62	Digital Globe
2006	O,C	1:19,270	600	0.88	University of Padua
2007	O,C	1:17,990	600	0.79	University of Padua
2009	O,C	1:17,280	1800	0.29	University of Padua
2010 (8 April)	GE,C			1.62	Digital Globe
2012	O,C			0.20	University of Padua
2015	GE,C			2.21	Digital Globe

[a]O, Ortho-photo; B/W, panchromatic; C, color; and GE, Google Earth 7™ image.

Each image was also subjected to a supervised pixel-based Maximum Likelihood Classification (MLC) [*Mather and Koch*, 2011] to reveal the spatial distribution of areas under three cover types (vegetation, bare ground, and water). The analysis was applied to the pixel sizes indicated in Table 1. Training data were carefully selected for each cover class within each image. Irregular polygons were used to select a large number of pixels in order to give a good representation of each class from which summary statistics could be extracted, because training data set selection can strongly affect the accuracy of the classification [*Hubert-Moy et al*., 2001; *Landgrebe*, 2003]. The original pixel size was retained for each classification because the accuracy of any classification is also influenced by the spatial resolution of the analyzed data [*Chen and Stow*, 2002].

Although bare ground was quite reliably classified, significant misclassification of water and vegetation occurred. Misclassification was mainly confined to the water-covered area, particularly where shadows from trees along the channel margin locally modified the pixel color within the water area. To solve this misclassification problem the margins of the wetted river channel area on each image were digitized and pixels within this water area were filtered so that those that had been classified as vegetation were reclassified as water. This provided a final classified image (e.g., Figure 2) which allowed the extent and spatial patterns in the vegetation cover and bare areas within the riparian corridor to be investigated.

The quality of the classification results was estimated both qualitatively (i.e., visually) and quantitatively through a confusion or error matrix [*Congalton*, 1994]. In the latter case, 30 points were investigated for each land cover class to assess the percentage of cases (pixels) classified correctly or incorrectly. This procedure was applied to classified images with and without the water mask. The overall accuracy and Kappa

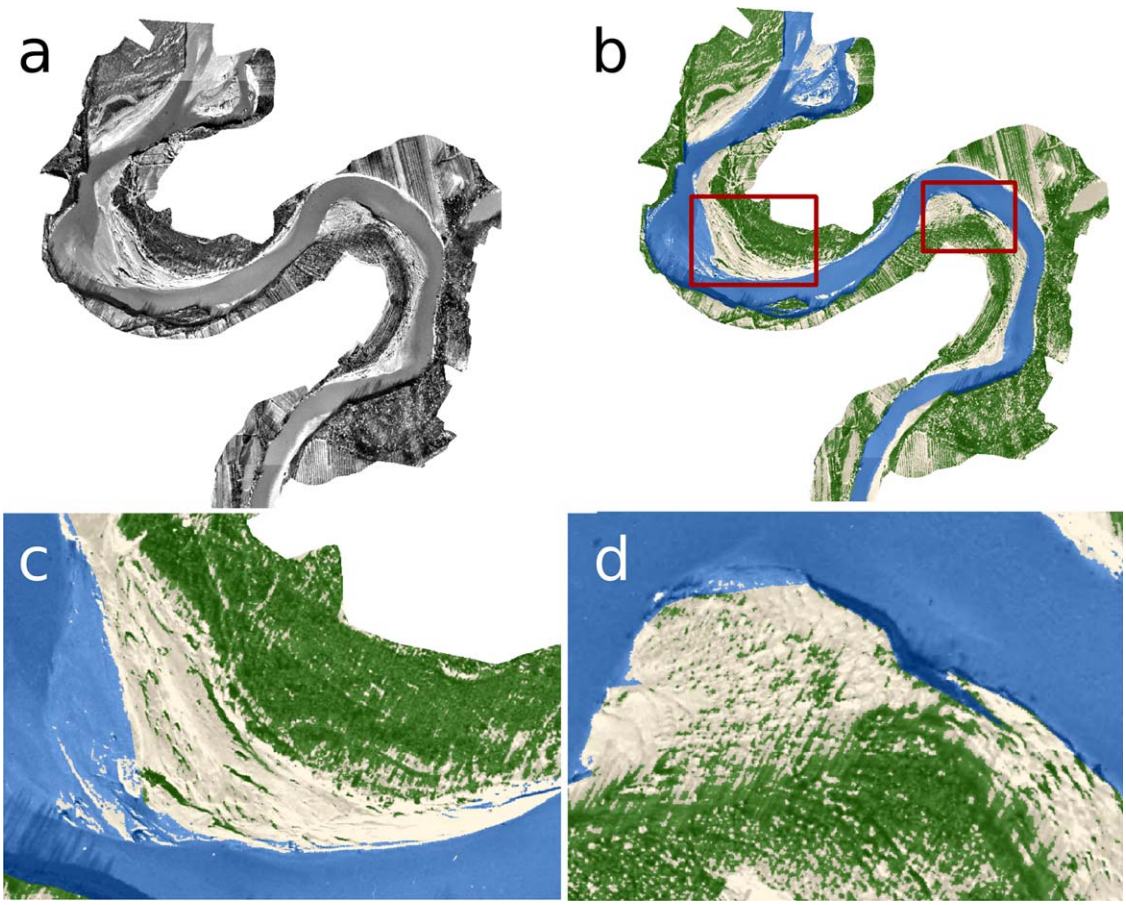

Figure 2. (a) Panchromatic photograph from 1966, (b) classified photograph to show vegetation (green), bare sediment (beige), and water (blue), (c) close-up of bend 3, and (d) close-up of bend 4.

parameter were estimated [*Congalton*, 1991; *Foody*, 2002] for each classification. Overall accuracy estimates can range from 0 (no points correctly classified) to 1 (all points correctly classified). Values of Kappa greater than 0.75 and less than 0.4 show, respectively, a "very good" or a "poor" classification performance [*Montserud and Leamans*, 1992; *Mather and Koch*, 2011]. Without a water mask, values of overall accuracy ranged from 0.58 to 0.97 (average = 0.78) and Kappa ranged from 0.34 to 0.95 (average = 0.68) but with the water mask the overall accuracy ranged from 0.84 to 1.00 (average = 0.95) and Kappa ranged from 0.77 to 1.00 (average = 0.92) indicating very satisfactory separation of vegetation and bare sediment beyond the water-filled channel and between sediment and water within the channel area, although some bare areas in shadow were misclassified as vegetation, particularly when panchromatic photographs were classified, as it is apparent in Figure 2.

The classified images represent not only different years but also different times of year and thus different stages of foliage development within the deciduous riparian forest. Therefore, the images could not be considered to represent a simple annual time sequence. Instead, following classification, each image was resampled to a standard grid (the average pixel size across the investigated images) and then reclassified to give vegetated pixels a value of 1 and all other pixels (bare sediment, water) a value of 0. The relevant sets of images (1983–2015 for bends 1 and 2, 1966–2001 for bends 3 and 4) were then overlain and summed to an aggregate map layer of vegetation persistence. For bends 1 and 2, the aggregate map layer displays values of 0 (never vegetated) to 11 (always vegetated) across eleven images from 1983 to 2015, whereas for bends 3 and 4 the aggregated map layer displays values of 0 to 6 spanning six images from 1966 to 2001. Lastly, because the channel had migrated laterally for more than one channel width over these two investigated time periods, the water-covered areas in the 2015 (bends 1 and 2) and 2001 (bends 3 and 4) images were used to mask those pixels whose vegetation cover reflected the transposition of pixels from one bank to the other (i.e., pixels that were initially vegetated on one bank, but then eroded during channel migration).

3.3. Field Observations

Two types of field data were collected to provide ground information about land surface form and vegetation cover. These data sets were collected at bend 1 during spring 2014.

The morphology of bend 1 was characterized by surveying a topographic transect across the river channel (A–A′, Figure 3f) using a total station and GPS. The total station was used to survey the surface beneath mature woodland where the vegetation cover prevented capture of a sufficient, consistent number of satellite signals, while the RTK GPS technique was used to survey all the points within the point bar or where the vegetation was sparse. Data from these two sources were merged using common control points surveyed using the rapid static GPS method with time interval ranges between 5 and 10 min. Very low flow during the field campaign allowed surveying of almost the entire channel cross section, excluding only the deepest part of the submerged channel bed. Within this deep region, a near-triangular bathymetry was estimated assuming scour at the outer bank and deposition on the inner bank to give a complete transverse profile of the river and its riparian margins.

Tree characteristics were estimated across the convex bank of bend 1 along transect A–A′, focusing on the dominant tree species, *P. nigra*, and the section of the convex bank under a continuous vegetation cover. Patches were selected to investigate tree characteristics on the alternating higher and lower areas of this undulating part of the surveyed transect. Rectangular quadrats were defined of a sufficient size (quadrat area varied from 40 to 200 m^2) to ensure representative sampling of patches of different tree size and density. Tree density was estimated by counting the total number of trees enclosed within each quadrat, and the diameter of each tree at 1 m above the ground surface was assigned to one of five diameter classes (class 1: $\leq$5 cm, class 2: 5–10 cm, class 3: 10–20 cm, class 4: 20–30 cm, and class 5: $>$30 cm). The height and trunk diameter (at 1 m above the ground surface) of the tallest tree in each quadrat was measured and a core was taken from the stem at 1 m above the ground surface, from which the age of the tree was estimated by counting the number of annual growth rings. These data were used to derive a growth curve that allowed approximate tree age at 1 m and height to be estimated from tree diameter. In addition, the vertical growth rate was estimated by dividing the height of the tree above the coring site by its estimated age.

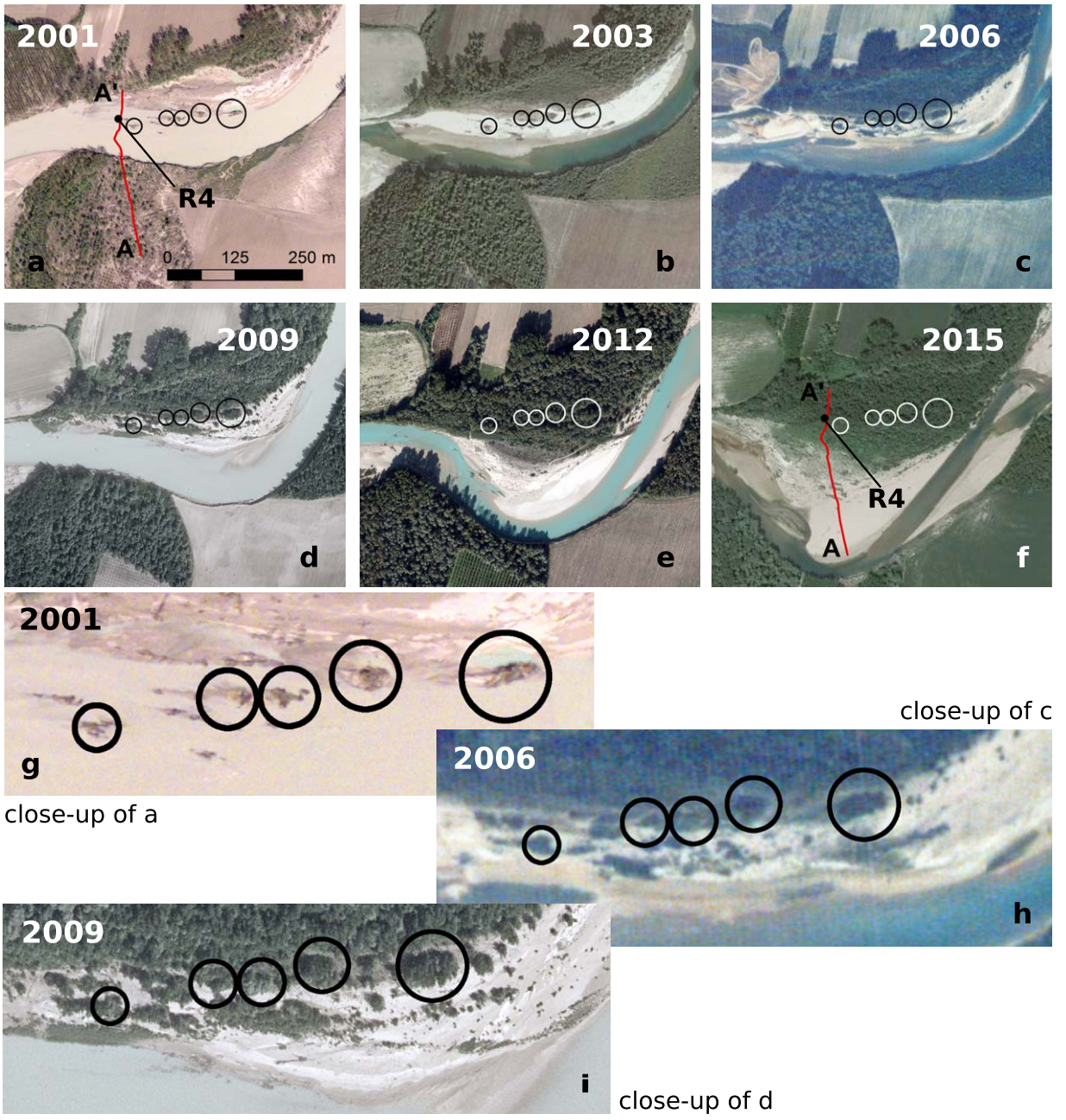

Figure 3. The positions of five trees (circles) deposited on bend 1, probably during the late 2000 flood, and their evolution observed in (a) 2001, (b) 2003, (c) 2006, (d) 2009, (e) 2012, and (f) 2015. Enlargements of the distribution of the five trees are provided for (g) 2001, (h) 2006, and (i) 2009. The circles vary in size to reflect differences in the size of the original deposited trees. The position of the surveyed transect A–A′ is shown along with that of the middle point of ridge R4 on the surveyed transect (Figure 5) in Figure 3f, close to the time of field survey, and in Figure 3a.

4. Results

4.1. Field and Image Evidence for the Role of Deposited Trees in Ridge-Swale Formation

The most reliable continuous water stage record for the middle to lower Tagliamento extends back to 1981 and comes from a gauge located 43 km upstream of the study site. This record indicates that the largest flood since 1981 occurred in late 2000 with other significant floods in 1990, 1996 (two floods), 2004, 2012, and 2014. A longer record of maximum annual water levels is available from a gauge located 67 km upstream of the study site, and this record shows the highest annual maximum water levels between 1886 and 2010 in 1966 and 2000 [*Ziliani and Surian*, 2012]. The 2000 event caused widespread erosion of riparian

trees, many of which were deposited on river bars during the flood's falling limb (Gurnell, contemporary field observation). Since the 1966 event was larger than the one in 2000, it undoubtedly also caused widespread tree erosion, transfer and deposition. These suggestions are supported by the 2001 image of bend 1 and the 1966 image of bend 3, which both show deposited trees (circles in Figures 3a, 3g, 4a, and 4e). It must be noted that, while circled features in Figure 4a are undoubtedly deposited trees, those in Figure 3a may also be visually interpreted as continuous patches of vegetation colonizing exposed sediments nearby

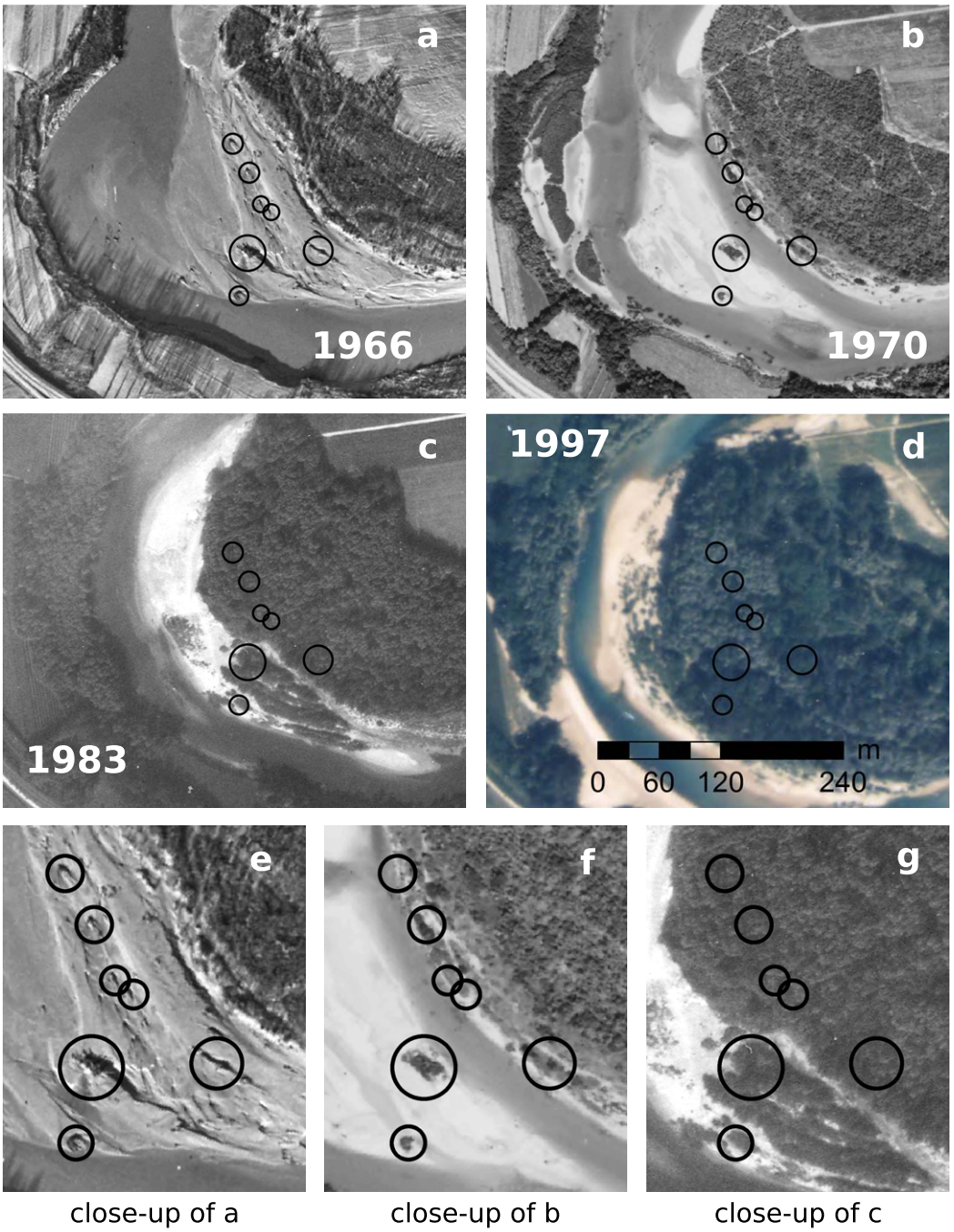

Figure 4. The positions of seven trees (circles) deposited on bend 3, probably during the 1966 flood, and their evolution observed in (a) 1966, (b) 1970, (c) 1983, and (d) 1997 (before the bend was stabilized). Enlargements of the distribution of the seven trees are provided for (e) 1966, (f) 1970, and (g) 1983. The circles vary in size to reflect differences in the size of the original deposited trees.

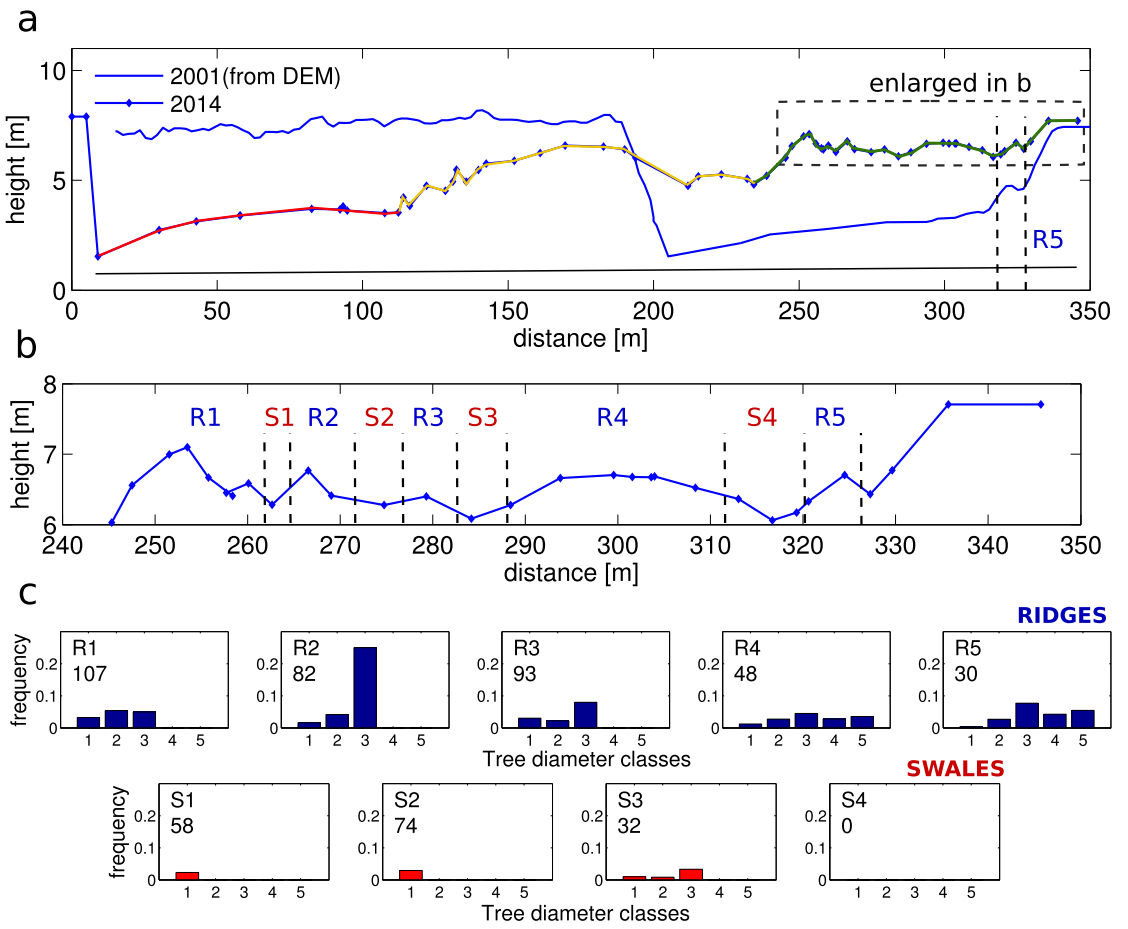

Figure 5. (a) Cross profile surveyed in 2014 overlain on the same cross profile in 2001, extracted from the 2001 DEM. For the 2014 cross profile, the red line indicates the unvegetated gravel area, the yellow line indicates an area under patchy vegetation, and the green line indicates the fully vegetated section of the inner bend in 2014, which is also indicated by the dashed box; (b) detailed cross profile of the vegetated section of the inner bend in 2014, showing a sequence of five ridges (R1–R5) with intervening swales (S1–S4); (c) relative frequencies of trees (*Populus nigra*) within five diameter classes on the five ridges and four swales (the number on each graph indicates the density of trees per 100 m^2).

deposited trees, which typically show analogous, elongated shapes [*Gurnell et al*., 2012]. Nevertheless, their location, far from the vegetated floodplain and close to the wet channel; their alignment along a hypothetical high flow streamline; and the decreasing spatial distribution of their size, further suggest their origin as deposited trees during a recent flood. Furthermore, sprouting trees deposited mainly on the upstream part of bend 3 can be seen in Figure 4d, which were probably transported by the 1996 floods. Vegetation growth around deposited trees and coalescence into vegetated strips around the inner bank of bends 1 and 3 can be observed in images following the 2000 (Figure 3a) and 1966 (Figure 4a) events, respectively, in Figures 3b–f and 4b–4d and are clearly visible in the enlargements shown in Figures 3h, 3i, 4f, and 4g. These illustrate that in both cases one long vegetated strip and at least one secondary strip developed around the original deposited trees. Also, as vegetation colonization and growth continued, the strips became incorporated into a continuous cover of riparian woodland. Both sets of images, but particularly the set in Figure 3, also illustrate later tree deposition and the development of additional vegetated strips on the channel side of the trees deposited earlier and highlighted by the sequence of circles in Figure 3a. For example, Figure 3c (see close-up in Figure 3h) shows several deposited, sprouting trees towards the edge of the inundated area, possibly deposited by the 2004 flood. These coalesce into a forked vegetated strip in Figure 3d, which becomes part of the area under continuous vegetation cover in Figures 3e and 3f.

When compared with the profile extracted from the 2001 DEM (Figure 5a), the 2014 surveyed transect shows that the channel's outer bank has migrated laterally more than 200 m between 2001 and 2014 and

the inner bank has aggraded significantly. The surveyed transect across the inner bank includes an unvegetated gravel area next to the low-flow channel (40–110 m: the red line in Figure 5a), an area of deposited, uprooted trees, pioneer islands and sparse colonizing vegetation retaining sand and finer sediments (110–140 m: left part of the yellow line) on the channel side of a patchily vegetated bar (140–200 m: right part of the yellow line) that is separated by a depression (200–240 m) from an undulating, continuously vegetated area (240–330 m: the green line).

Tree characteristics were investigated within the continuously vegetated area (dashed box, Figure 5a), which shows distinct ridges with intervening depressions or swales (Figure 5b), with an average lateral spacing of 5–10 m, except for ridge R4 which is wider than 20 m. Sand and finer sediments characterize the surface of this entire area. These finer sediments, probably underlain by gravels, are deposited on the 2001 point bar (Figure 5a). The process of sand and finer sediment retention around vegetation is observed on the central sparsely vegetated area of the inner bank on the surveyed profile (110–200 m, yellow line in Figure 5a). Trees within the continuously vegetated area are almost entirely *P. nigra*, and bar graphs (Figure 5c) of their relative size frequency across five trunk diameter classes on the ridges (R1–R5) and intervening swales (S1–S4) show increasing tree diameter and a decreasing number of trees per unit area with distance from the river; larger but also more densely spaced trees on the ridges than in the swales; and only trees from the smallest diameter class present in swales S1 and S2. A simple linear regression relationship between tree height (in m) and tree diameter at 1 m (in cm) estimated from measurements of the largest one or two trees in each quadrat (height $= 2.85 + 0.67 \times$ diameter, $R^2 = 0.902$, $n = 11$) indicates an increase in tree height across the diameter classes such that classes 1, 2, 3, 4, and 5 represent, respectively, a height of 4, 7, 12, 20, and 21 m.

The ages of the largest trees on each of the ridges were computed at ground level from the count of annual rings at 1 m and each tree's average annual vertical growth rate. The estimated ages were 5, 6, 8, 15, and 20 years for R1, R2, R3, R4, and R5, respectively. In addition to uncertainty in these estimates resulting from possible failure to identify some annual growth rings or counting of "false" rings, each of these trees is likely to be older than these estimates because of aggradation of the ground surface above the original gravel bar surface at the time of deposition as the trees have grown. Nevertheless, the 2001 cross profile (Figure 5a) indicates that a ridge was present at the horizontal location of R5 at that time, indicating the presence of sediment-retaining trees that pre-date the 2000 flood, and thus probably relate to the 1996 floods. Given dating uncertainties and the proximity of R4 to the deposited trees observed in the 2001 image (Figure 3), it seems likely that R4, the widest continuously vegetated ridge, is the downstream tail of a ridge initiated by 2000 flood-deposited trees. The remaining ridges (R1–R3) have a smaller lateral extent and their origin postdates the 2000 flood. As noted above, the 2006 air photograph shows widespread sprouting deposited trees that were incorporated into vegetated strips and thus later scroll and ridge development (Figure 3), suggesting that R1–R3 probably date to the 2004 flood or possibly a little later. The smaller (younger) tree cover in the swales within the continuously vegetated area indicates vegetation colonization of the swales after the adjacent ridges. Furthermore, if the most recent ridges within the continuously vegetated area in 2014 date back to the 2004 flood, the area covered by deposited trees, pioneer islands and sparse patches of colonizing vegetation (110–140 m, Figure 5a) has developed its vegetation cover since the 2004 flood or possibly even more recently.

4.2. Associations Between Vegetation and Topography on the Convex Banks of Four Meander Bends

Figure 6 refers to bends 1 and 2, which remain freely migrating (bend 1) or subject to stabilization only recently (bend 2). The active river channel is well defined in the DEM derived from the LiDAR data (Figure 6a) by an almost homogeneous yellow color. Focusing on the riparian area, ridges running parallel to the edge of the convex bends are clearly evident. These ridges indicate scroll bars that evolve, with increasing age, into ridge and swale topography as the meanders migrate. The increasing age of the ridges with distance from the water-filled channel is indicated by the bands of trees of increasing height captured by the CHM (Canopy Height Model, Figure 6b). Close-ups of the DEM and CHM illustrate the correspondence of taller (older) tree canopies with ridges that are at a greater distance from the water-filled channel. This correspondence is confirmed by Figure 6d, which shows a histogram (bars) of the relative frequency of pixels of different surface elevation in relation to the frequency of occurrence of vegetation canopies of different heights (ages) on pixels falling within each of the elevation bands. Areas between 4 and 5.2 m elevation are mainly covered by bare ground or short vegetation (<5 m), areas between 5.2 and 6.2 m elevation are

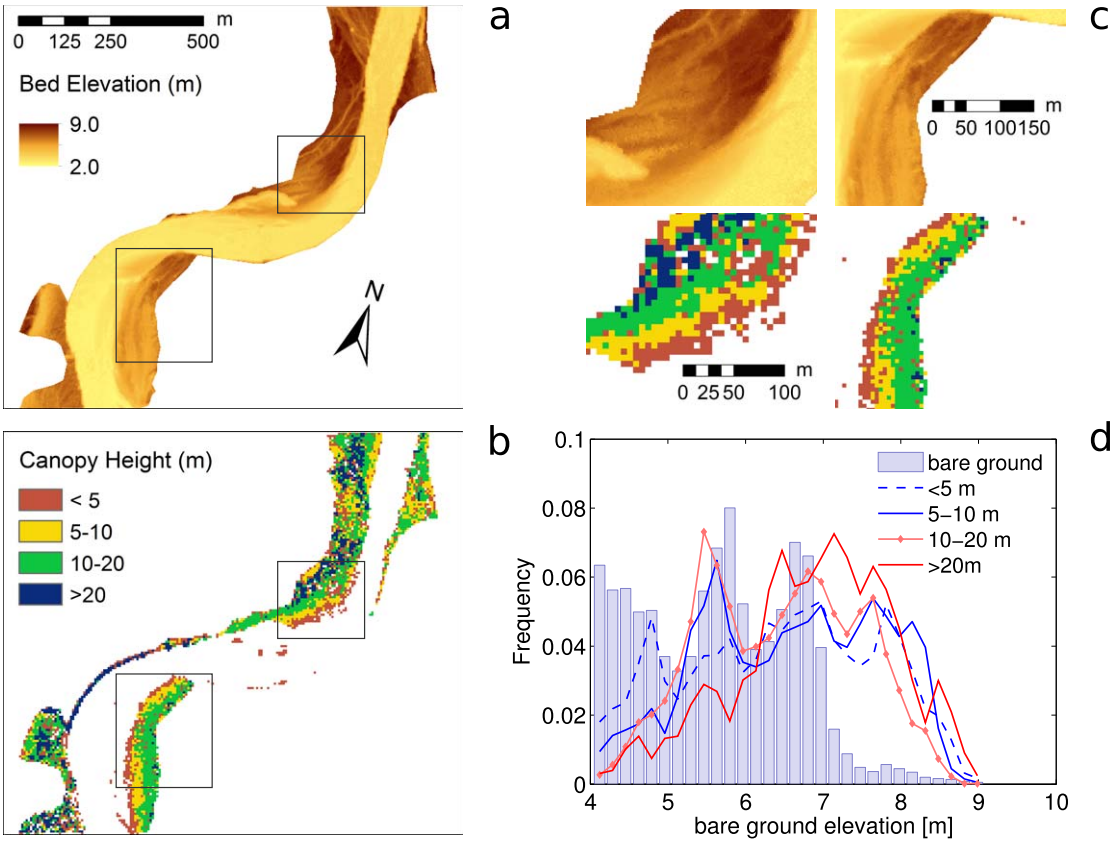

Figure 6. (a) The DEM and (b) the CHM extracted from the 2001 LiDAR survey for bends 1 and 2 (Figure 1b) and the portion of the floodplain naturally colonized by riparian woodland at the survey date; (c) enlargements of the DEM and CHM for the inner banks of bends 1 and 2 (locations indicated by boxes in Figure 6b; (d) distributions of the relative frequency of vegetation canopy height classes (lines) in relation to ground surface elevation above 4 m (bars) in the area shown in Figure 6a.

dominated by vegetation that is 10–20 m tall and the most frequent height class for vegetation at elevations over 6.2 m is >20 m. The fact that all canopy height frequency curves persist at higher elevations reflects the low leaf cover at the time of the LiDAR survey (April), which permitted deep penetration through the canopy to lower branches, even though the trees are predominantly tall and densely spaced.

Analysis of the classified images to assess vegetation persistence provides a second perspective on riparian woodland age and structure, which can be compared with the ground topography from the LiDAR analysis (Figure 7a). Focusing again on bends 1 and 2, two vegetation persistence maps were produced: the first summarizes vegetation persistence across four images spanning the period from 1983 to 2001, to match the date of the LiDAR survey (Figure 7b), and the second integrates 11 images spanning the period 1983–2015 (Figure 7c). Here dates are different from those presented in section 3 because 1983 is the earliest date within the data set for which bend 1 and 2 had started their development, while bends 3 and 4 were already well developed in the earlier images from 1966. Both persistence maps show the number of images in which each pixel was classified as being vegetated. For Figure 7b, vegetation persistence is only displayed for those pixels under naturally colonized riparian vegetation at the time of the 2001 survey. The crests of scrolls and ridges identified by the DEM (Figure 7a) are superimposed (black lines) on the 1983–2001 vegetation persistence map (Figure 7b) in the areas shown in the enlargements, and some of them show a consistent overlap with the edge separating areas having different vegetation persistence values. The identified strips present an almost constant width around 20 and 16 m for bends 1 and 2, respectively. The enlargement in Figure 7c illustrates a complex of linear areas of each vegetation persistence category, corresponding to strips of vegetation of increasing persistence and age with distance from the wetted channel. Near to the channel these features are smaller and patchier, indicative of recently deposited trees and pioneer islands. Moreover, Figure 7c shows wider vegetated bands compared to those observed in Figure 7b, with young plants organized in strips 2 or 3 times larger than the oldest plants. This may be related

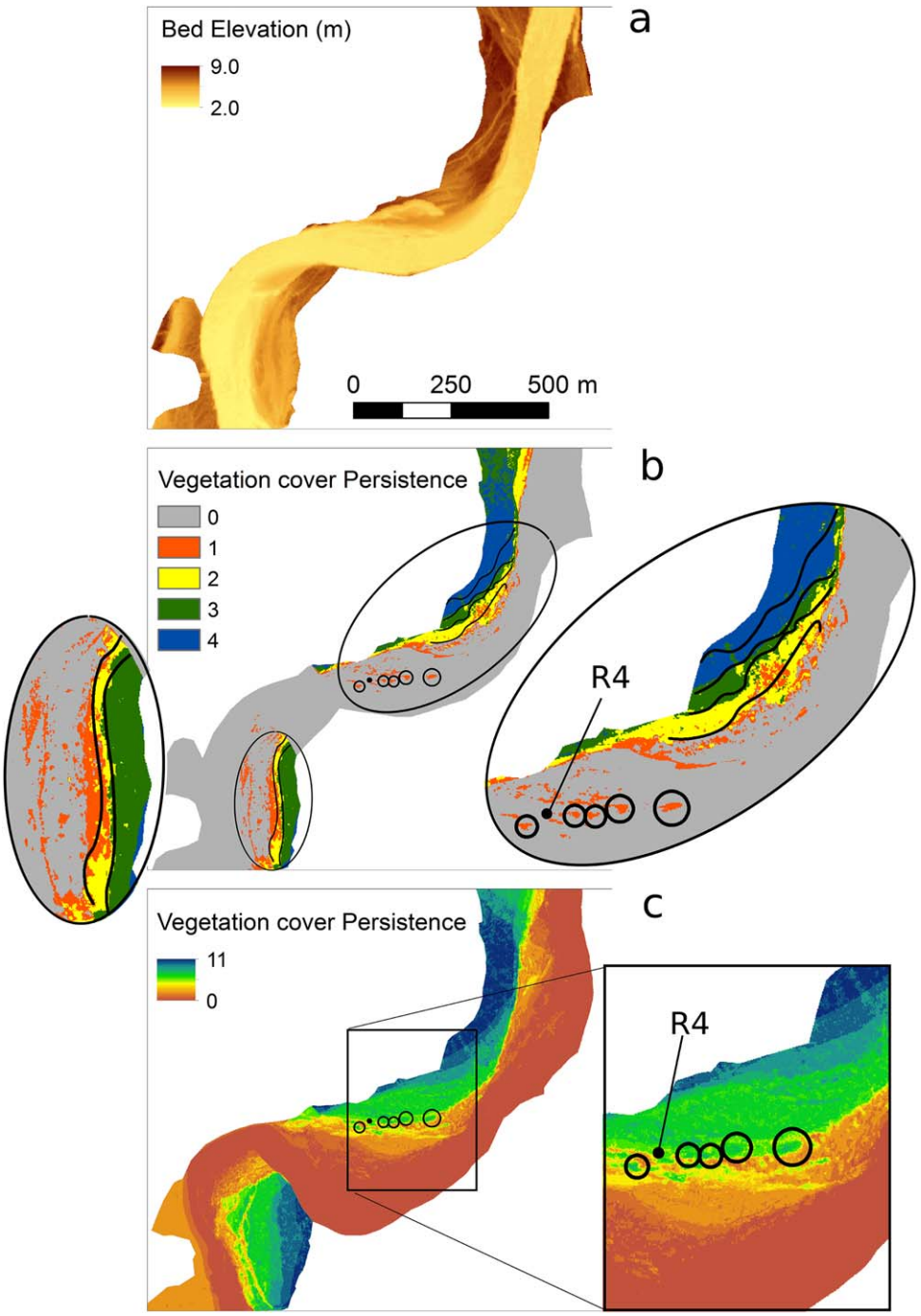

Figure 7. (a) DEM and vegetation cover persistence map within the natural riparian area for the period (b) 1983–2001 and (c) 1983–2015. The black continuous lines represent the positions of swales observed from the DEM (Figure 7a), the circles indicate the deposited trees observed in the 2001 image (Figure 3a) and the dot indicates the mid-point of the local extension of ridge R4 (Figure 3a).

to an increase in the lateral migration rate of bend 1 after 2009 (see Figure 3). Finally, the position of the deposited trees in 2001 and of ridge R4 (extended upstream from the surveyed cross section) are indicated in both persistence maps (Figures 7b and 7c). This shows how, during meander bend evolution, the stranded trees coalesced into a strip of continuous vegetation whose position corresponds with that of ridge R4 (Figure 7c). Interestingly, the deposited trees are almost perfectly aligned along the edge between areas with vegetation persistence through 4 (yellow) and 5–6 consecutive images (green).

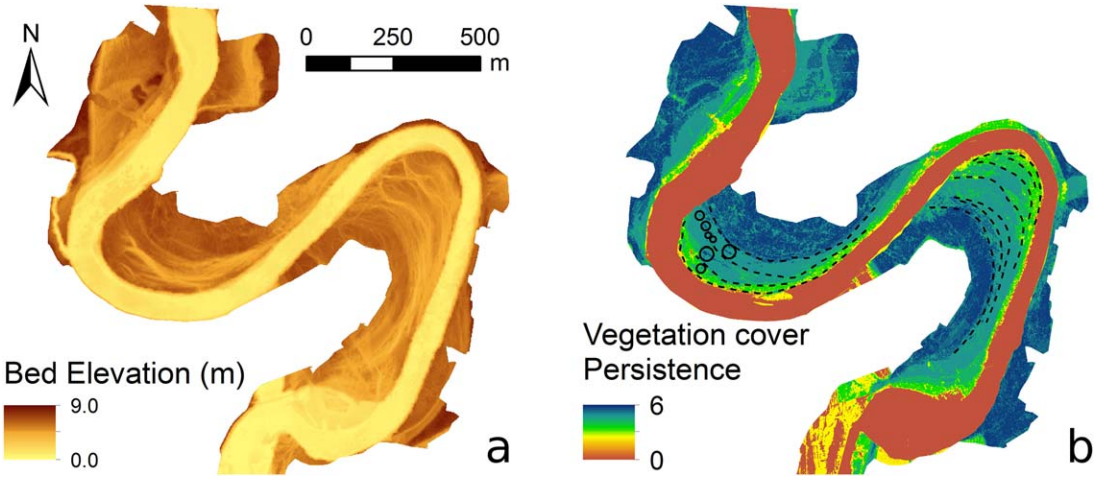

Figure 8. (a) DEM and (b) vegetation cover persistence map for the period 1966–2001 for bends 3 and 4 (Figure 1c). The dashed lines show the position of the swales extracted from the DEM (Figure 8a), the circles indicate the positions of deposited trees observed in the 1966 image (Figure 4a).

The 2001 DEM (Figure 8a) and the vegetation persistence map from 1966 to 2001 (Figure 8b) for downstream bends 3 and 4 refer to the period before these bends were stabilized. A consistent streamwise alignment of swales developed in the advancing floodplain of bends 3 and 4 (extracted from Figure 8a) and the edges of curvilinear strips with the same vegetation persistence values (Figure 8b) provide further evidence of the spatial association between riparian tree growth and the topographical ridge-swale pattern. The width of the vegetated ridges within bend 3 is about 40 m, and it decreases to about 25 m for the ridges closest to the channel margin. In bend 4, homogeneous vegetation patterns are organized along analogous curvilinear strips that are 25–30 m wide both near and far from the channel and are about 60 m wide in the middle sections of the inner bank.

5. Discussion

5.1. The Role of Trees in Scrolls, Ridge, and Swale Formation Along the Lower Tagliamento River

The combined analysis of information extracted from historical images and LiDAR data has revealed (i) the appearance of deposited trees and elongated vegetated patches following known flood events; (ii) temporal progression from deposited trees, through small to larger elongated vegetated patches (pioneer islands), to their coalescence into long, curvilinear vegetated features that eventually become absorbed into the continuous vegetation cover of the riparian forest; and (iii) a spatial correspondence between ridge and swale topography and tree cover development and persistence. Field survey has also shown: the presence of a deep chute that separates the inner bank into two higher elevated areas; a high point bar area where the ground presents small oscillations related to the sedimentation induced by pioneer plants and stranded trees during floods; and a developing floodplain area, which is located far from the main channel and is characterized by an undulating surface with vegetated ridges and almost bare swales.

This analysis of convex bends on the lower Tagliamento River has also produced approximate (indicative) dates for the formation of ridge and swale features. Floods that have deposited trees and initiated scroll development appear to have occurred in 1966, 1996, 2000, 2004, and also more recently, indicating an irregular, quasi-decadal frequency of scroll, ridge, and swale initiation that concurs with the lower limit of the likely time scales proposed by *Bridge et al*. [1995].

While deposited trees appear to perform a key role in the initiation of scrolls on the lower Tagliamento meanders, subsequent trapping of additional wood pieces and seeds along with sand and finer sediments help to quickly create a diverse vegetation cover on the evolving pioneer islands [e.g., *Francis et al*., 2008] and thus also to contribute to vegetation roughness and scroll development as suggested by *Hickin* [1984].

Observations on the four examined bends reveal that the ridge-swale pattern creates an undulating floodplain ground surface with fairly regular oscillations locally oriented orthogonal to the meandering channel

centerline. These oscillations display a range of different wavelengths (i.e., distances between two consecutive ridges or swales), ranging from a few meters (i.e., the space needed to accommodate just one plant on top of the ridge) to around 60 m (i.e., the typical width of the permanently wet low-flow channel). In most bends, the crests of ridges and troughs of swales are systematically aligned with the curvilinear strips of vegetation persistence extracted from the aerial images.

5.2. A Conceptual Model of Mechanisms of Scroll Bar and Ridge-Swale Formation Along Meandering Rivers

Observations presented in this paper support previous field observations of the development of scrolls on meander bends, in particular further linking their formation to the evolution of riparian vegetation. In the case of the Tagliamento River, riparian vegetation development is mainly initiated by the regeneration of uprooted, flood-deposited riparian trees supplemented by the growth of plants from both seeds and vegetative fragments. Nevertheless, recent laboratory experiments have shown that scrolls may also form in the complete absence of wood or vegetation [e.g., *van de Lageweg et al*., 2015]. Thus, wood and vegetation may not be a necessary prerequisite for scroll formation, but there is increasing evidence from other river systems and other nonmeandering reaches of the Tagliamento that they are likely to be important contributory factors.

i. Observations from braided reaches of the Tagliamento have revealed flood deposition of uprooted trees during the falling limb of floods across elevation bands that are narrower than the range provided by the bed topography [*Bertoldi et al*., 2013]. In other words, wood is deposited across a strand zone or area rather than a strand line. Such a strand zone provides an elongated band across which relatively broad ridges might aggrade on the point bars of meander bends.
ii. Once deposited, the downstream extension of deposited tree features through the formation of tail bars [*Kleinhans and van den Berg*, 2011] is widely observed and forms a first stage in sediment retention.
iii. Upstream and downstream extension of such features have also been observed through their complete burial by alluvial sediment [*Nanson*, 1981] or through additional wood retention around the upstream-facing root wad and then gradual aggradation around tree seedlings germinating on the wood piles [*Abbe and Montgomery*, 1996].
iv. Upstream, downstream, and some lateral extension of these features can be rapid when a vegetation canopy generated from seedlings [*McKenney et al*., 1995] or sprouting wood [*Gurnell et al*., 2001] traps sediment. Where the features have developed from a linear strand zone, their coalescence results in the development of linear (scroll) bars.

The present observations support further development and refinement of the conceptual model of inner bank accretion proposed by *McKenney et al*. [1995], incorporating processes of scroll bar formation within the newly forming floodplain initiated by uprooted trees deposited on the point bar. We argue that an important step is the transformation of observed small-scale scroll bars into fully developed, larger-scale ridge and swale oscillations during the lateral advance of the inner bank. We illustrate our conceptual model according to a seven-stage chronological sequence (Figure 9).

Stage I. Deposition of an uprooted tree on a point bar is followed by spatially selective deposition of finer sediments associated with the wake and shear layers that locally reduce flow strength along a downstream path that is approximately aligned with the tree. Evidence of such processes has been provided for braid bars [*Gurnell et al*., 2001], and the deposition patterns can be also visually inferred from Figure 3a, downstream of the deposited trees.
Stage II. By retaining moisture and nutrients, these finer sediment deposits promote root and shoot development from the deposited tree during low flow (Figure 9a).
Stage III. If sufficiently anchored to avoid remobilization, the sprouting tree alters the scour-deposition pattern during inundating flows [*Abbe and Montgomery*, 1996; *Kleinhans and van den Berg*, 2011]. In this way, spatially selective deposition of transported sediments promotes formation of oscillations of the ground surface (scrolls) that are approximately aligned with local streamlines, particularly during flow recession.
Stage IV. The process of tree growth, flow modification and sediment scour-deposition is repeated through subsequent low flow and inundation events, contributing to overall sediment deposition on the point bar, the main driving mechanism of advancement of the inner bank.

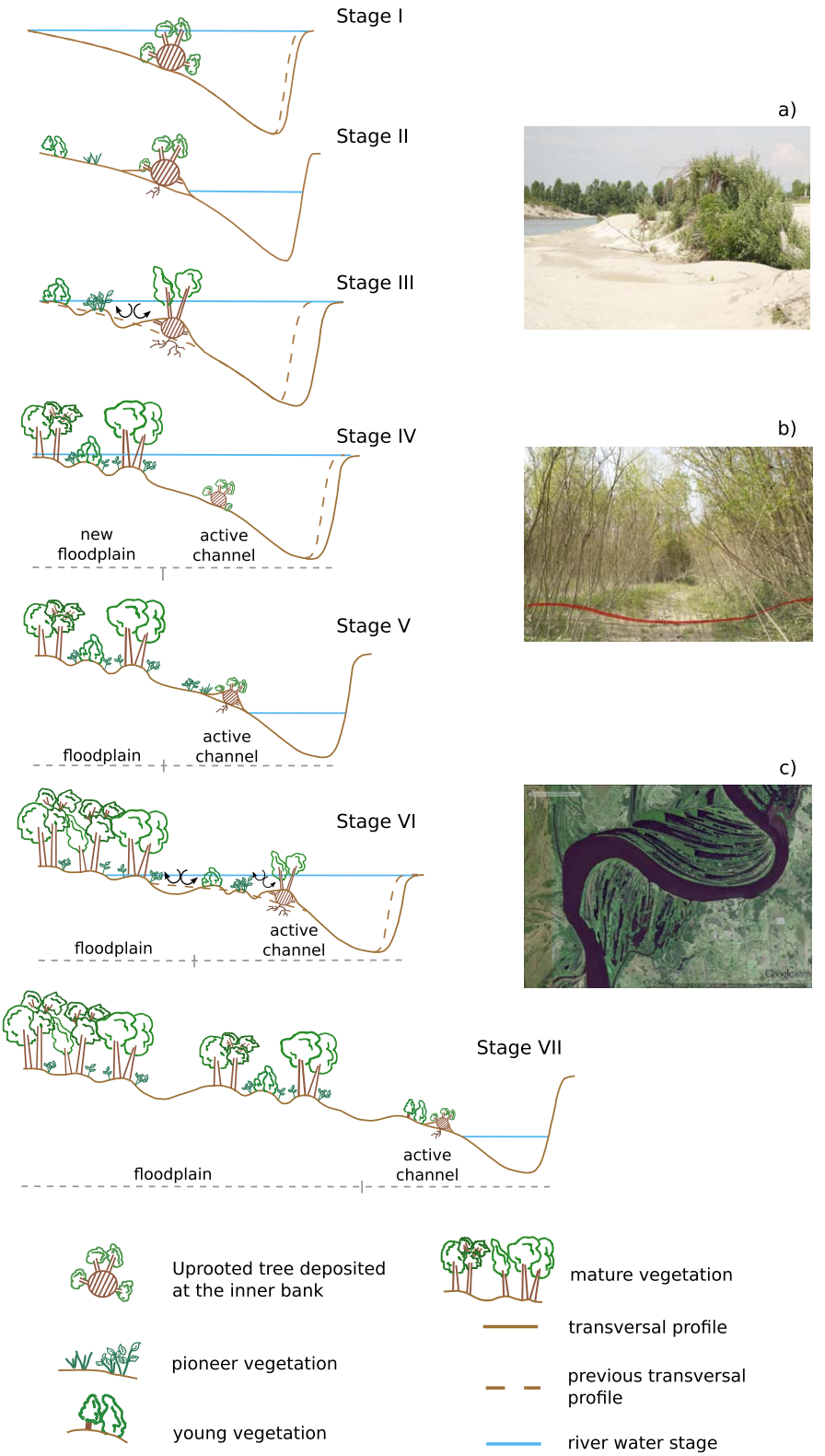

Figure 9. A seven-stage conceptual model of mechanisms of scroll bar and ridge-swale development in the lateral evolution of meander bends. When present, dashed lines denote the position of the outer bank at the previous model stage. The images provide examples of (a) a deposited, sprouting tree buried by fine sediment on the point bar of bend 1 of the Tagliamento River; (b) a lateral sequence of vegetated ridges and unvegetated swales on bend 1 of the Tagliamento River; and (c) ridges and swales of the Rio Paraguay, Paraguay (*Source*: digital globe for Google Earth).

Stage V. Deposition of new uprooted trees by major floods (stage IV) leads to the development of new scrolls and the initiation of ridge-swale sequences on the surface of the advancing point bar, which approximately keeps pace with retreat of the opposite bank, although with a temporal delay related to the degree of oscillation of the local active channel width. Different rates of lateral movement may be reflected in different lateral spacing of ridges and swales. Vegetation development on the corrugated bar surface results in consolidation of the ridge-swale sequence.
Stage VI. Vegetation development on the ridges self-protects them from the action of high flows, inducing preferential sediment deposition on the ridges and scour of the intervening bare swale areas. The intensity of these processes decreases with increasing surface elevation (increasingly above most flood disturbances) and lateral distance from the main channel (as the bend migrates), so that the undulating pattern of the ground topography is preserved but vegetation colonization of the swales commences.
Stage VII. Eventually, possibly initiated by a large flood, some of the small-scale ridges and swales may coalesce as a result of broader scale sedimentation encompassing several ridges and swales. Such a process would concentrate most of the flow along the inner bank, leading to sets of ridges and swales being subjected to differential or no sediment deposition.

These mechanisms could generate groups of ridges and swales evolving in a similar way to the individual scrolls in stage III but organized at a larger spatial scale, with each ridge crest characterized by several small oscillations initiated from individual deposited plants (stage VII) that has been preserved during bank evolution (Figure 9b). According to this model, during the lateral migration of a meander bend, the initial sequences of scrolls, ridges, and swales on the point bar may evolve and coalesce to form larger-scale ridges, eventually determining a vegetation-topography coevolution that produces the floodplain ridges and swales that are often clearly detectable in aerial or satellite images of migrating, meandering rivers (Figure 9c).

5.3. Topography-Vegetation Association: Implications for Meander Biomorphodynamic Modeling

Results obtained through this historical analysis can inform modeling research that aims to describe the biomorphodynamics of meandering rivers using physically based relations. Modeling of meander bend evolution has been traditionally based on mathematical equations that essentially account for the dynamics of sediment transport in the channel and only provide a very simplified representation of the bank dynamics [*Seminara*, 2006], perhaps with more accurate modeling of bank erosion compared with bank accretion [*Guneralp et al*., 2012]. The mutual interaction between floodplain vegetation and river channel morphodynamics has been investigated only recently in order to understand the effects on meander planform evolution [*Perucca et al*., 2006, 2007] and to explore the influence of vegetation on river morphology [*van Oorschot et al*., 2016], with other recent examples focusing on the development of river bars under unsteady flow conditions [*Bertoldi et al*., 2014]. The numerical model of *Nicholas* [2013] displays scroll bar formation on a simulated floodplain by imposing simplified rules whereby the active channel computational cells are transformed into floodplain cells that are more resistant to fluvial erosion if they remain dry or if they are subject to a water depth smaller than an imposed threshold within a specified interval of time. In this case, the progressive development of scrolls at each overbank flow gives rise to the point bar.

Observations presented in this paper reveal the fundamental role that can be played by uprooted, deposited trees in initiating scrolls, which are eventually incorporated into the floodplain as sequences of ridges and swales. Such a mechanism probably needs to be considered to improve existing coupled vegetation-morphodynamic models [e.g., *Camporeale et al*., 2007; *Marani et al*., 2013; *Solari et al*., 2016], whose level of detail is as yet too coarse for an explicit inclusion of such a process. A promising path in this direction might be to build on the coupled model for river hydrodynamics and large wood transport recently proposed by *Ruiz-Villanueva et al*. [2016], in order to relate wood deposition to river flow and channel morphology, initially without exploring the feedback of the deposited wood on channel bed morphological evolution. A parameterized version of such flow-wood-morphology dynamics might also be incorporated into more simplified, lumped biomorphodynamic models, such as the one proposed by *Zen et al*. [2016], to investigate the role of biological and hydrological factors in the lateral accretion of the inner bank of meander bends. In their analysis, *Zen et al*. [2016] show that the mutual interaction between water flow (associated with fluctuations in water stage) and the riparian vegetation is crucial for the initiation of scrolls, and by providing a quantitative description of the lateral accretion of the inner bank, their work constitutes a first attempt to investigate the spatial and temporal scales that govern the lateral evolution of meandering channels.

6. Conclusions

Historical analysis of secondary sources is an invaluable way of extending geomorphological investigations back over long time periods. In the present research, a combined analysis of contemporary field observations, historical images, and river stage time series has been used to advance present understanding of the evolution of geomorphological features that may take a decade or more to develop. The analysis has revealed a clear relation between the ridge and swale topography of the inner bank and vegetation structure and persistence, further supporting the fact that deposited trees and wood can contribute to scroll initiation on the convex bank of meander bends. Based on this, we proposed a conceptual model to explain the mechanisms that, through the mutual interaction between channel morphogenesis and vegetation, generate scrolls, ridges, and swales on the inner bank of vegetated meander bends. In particular, the model attempts to elucidate how such morphological features can evolve and can become organized on a larger scale to create the ridge and swale topography that characterizes the floodplains of many naturally meandering rivers.

Results from this work can inform modeling activities aimed at describing the lateral migration of the inner bank and the vertical aggradation of the floodplain associated with the planform evolution of river meanders.

Because the newly created floodplain of the Tagliamento River is rapidly converted into agricultural fields, it is hard to detect longer term floodplain evolution. Nevertheless, large scale ridge and swale features can often be seen from satellite images (i.e., with a spacing approximating the wetted channel width). Unfortunately, the resolution of such images together with the high dynamicity that distinguishes such types of river does not permit detailed detection of landforms being initiated by riparian vegetation in the way and at the scale documented in this paper. Therefore, a future challenge is to collect detailed information at small and large spatial scales to reconstruct the long term evolution of floodplain surfaces and the precise role of vegetation in this process. This will provide insights into the mechanisms we have proposed and the potential to explore the applicability of the conceptual model to other river systems.

Acknowledgments

The data used in the analysis and to support the discussion are available upon request to the corresponding author. The authors thank Bruce Rhoads, Kory Konsoer, and Gerald Nanson for their suggestions that contributed in improving the quality of the work. The work of S. Zen has been supported by Project ETSCH2000 funded by the Autonomous Province of Bolzano, Italy, and by the SMART Joint Doctoral Program (Science for Management of Rivers and Their Tidal Systems), which is financed by the Erasmus Mundus Program of the European Union, FPA-0024–2011. There are no conflicts of interest for any author involved in the work.

References

Abbe, T. B., and D. R. Montgomery (1996), Large woody debris jams, channel hydraulics and habitat formation in large rivers, *Reg. Rivers Res. Manage.*, *12*(2–3), 201–221.

Antonarakis, A. S., K. S. Richards, and J. Brasington (2008), Object-based land cover classification using airborne LiDAR, *Remote Sens. Environ.*, *112*, 2988–2998, doi:10.1016/j.rse.2008.02.004.

Bagnold, R. (1960), Some aspects of the shape of river meanders, *U.S. Geol. Surv. Prof. Pap.*, *282E*, 135–144.

Bertoldi, W., A. M. Gurnell, and N. A. Drake (2011), The topographic signature of vegetation development along a braided river: Results of a combined analysis of airborne LiDAR, colour air photographs and ground measurements, *Water Resour. Res.*, *47*, W06525, doi:10.1029/2010WR010319.

Bertoldi, W., A. M. Gurnell, and M. Welber (2013), Wood recruitment and retention: The fate of eroded trees on a braided river explored using a combination of field and remotely-sensed data sources, *Geomorphology*, *180–181*(1), 146–155.

Bertoldi, W., A. Siviglia, S. Tettamanti, M. Toffolon, D. Vetsch, and S. Francalanci (2014), Modeling vegetation controls on fluvial morphological trajectories, *Geophys. Res. Lett.*, *41*, 7167–7175, doi:10.1002/2014GL061666.

Bizzi, S., L. Demarchi, R. C. Grabowski, C. J. Weissteiner, and W. Van de Bund (2016), The use of remote sensing to characterise hydromorphological properties of European rivers, *Aquat. Sci.*, *78*, 57–70, doi:10.1007/s00027-015-0430-7.

Blanckaert, K., M. G. Kleinhans, S. J. McLelland, W. S. J. Uijttewaal, B. J. Murphy, A. van de Kruijs, D. R. Parsons, and Q. Chen (2013), Flow separation at the inner (convex) and outer (concave) banks of constant-width and widening open-channel bends, *Earth Surf. Processes Landforms*, *38*(7), 696–716.

Bridge, J. S., J. A. N. Alexander, R. E. L. Collier, R. L. Gawthorpe, and J. Jarvis (1995), Ground-penetrating radar and coring used to study the large-scale structure of point-bar deposits in three dimensions, *Sedimentology*, *42*(6), 839–852.

Carbonneau, P., and H. Piégay (2012), *Fluvial Remote Sensing for Science and Management*, John Wiley, Chichester, U. K.

Carbonneau, P., M. A. Fonstad, W.A. Marcus, and S. J. Dugdale (2012), Making riverscapes real, *Geomorphology*, *137*, 74–86, doi:10.1016/j.geomorph.2010.09.030.

Camporeale, C., P. Perona, A. Porporato, and L. Ridolfi (2007), Hierarchy of models for meandering rivers and related morphodynamic processes, *Rev. Geophys.*, *45*, RG1001, doi:10.1029/2005RG000185.

Chen, D. M., and D. Stow (2002), The effect of training strategies on supervised classification at different spatial resolutions, *Photogramm. Eng. Remote Sens.*, *68*, 1155–1161.

Colonnello, G. (1990), A Venezuelan floodplain study on the Orinoco River, *For. Ecol. Manage.*, *33/34*, 103–124.

Congalton, R. G. (1991), A review of assessing the accuracy of classifications of remotely sensed data, *Remote Sens. Environ.*, *37*, 35–46.

Congalton, R. G. (1994), Accuracy assessment of remotely sensed data: Future needs and directions, in *Proceedings of Pecora 12 Land Information From Space-Based Systems*, pp. 383–388, ASPRS, Bethesda, Md.

Dufour, S., I. Bernez, J. Betbeder, S. Corgne, L. Hubert-Moy, J. Nabucet, S. Rapinel, J. Sawtschuk, and C. Trollé (2013), Monitoring restored riparian vegetation: How can recent developments in remote sensing sciences help?, *Knowledge Manage. Aquat. Ecosyst.*, *410*, 10, doi:10.1051/kmae/2013068.

Fonstad, M. A., and W. A. Marcus (2010), High resolution, basin extent observations and implications for understanding river form and process, *Earth Surf. Process. Landforms*, *35*, 680–698, doi:10.1002/esp.1969.

Foody, G. M. (2002), Status of land cover classification accuracy assessment, *Remote Sens. Environ.*, *80*, 185–201.
Francis, R. A., P. Tibaldeschi, and L. McDougall (2008), Fluvially-deposited large wood and riparian plant diversity, *Wetlands Ecol. Manage.*, *16*(5), 371–382.
Grabowski, R. C., and A. M. Gurnell (2016), Hydrogeomorphology—Ecology interactions in river systems, *River Res. Appl.*, *32*, 139–141, doi: 10.1002/rra.2974.
Grabowski, R. C., N. Surian, and A. M. Gurnell (2014), Characterizing geomorphological change to support sustainable river restoration and management, *WIREs Water*, *1*, 483–512, doi:10.1002/wat2.1037.
Grenfell, M., R. Aalto, and A. Nicholas (2012), Chute channel dynamics in large, sand-bed meandering rivers, *Earth Surf. Processes Landforms*, *37*(3), 315–331.
Guneralp, I., J. D. Abad, G. Zolezzi, and J. Hooke (2012), Advances and challenges in meandering channels research, *Geomorphology*, *163–164*, 1–9.
Gurnell, A., and G. Petts (2006), Trees as riparian engineers: The Tagliamento River, Italy, *Earth Surf. Processes Landforms*, *31*(12), 1558–1574.
Gurnell, A. M., G. E. Petts, N. Harris, J. V. Ward, K. Tockner, P. J. Edwards, and J. Kollmann (2000), Large wood retention in river channels: The case of the Fiume Tagliamento, Italy, *Earth Surf. Processes Landforms*, *25*(3), 255–275.
Gurnell, A. M., G. E. Petts, D. M. Hannah, B. P. G. Smith, P. J. Edwards, J. Kollmann, J. V. Ward, and K. Tockner (2001), Riparian vegetation and island formation along the gravel-bed Fiume Tagliamento, Italy, *Earth Surf. Processes Landforms*, *26*(1), 31–62.
Gurnell, A. M., W. Bertoldi, and D. Corenblit (2012), Changing river channels: The roles of hydrological processes, plants and pioneer fluvial landforms in humid temperate, mixed load, gravel bed rivers, *Earth Sci. Rev.*, *111*(1), 129–141.
Hickin, E. J. (1974), The development of river meanders in natural river channels, *Am. J. Sci.*, *274*, 414–442.
Hickin, E. J. (1984), Vegetation and river channel dynamics, *Can. Geogr.*, *28*, 111–126.
Hollaus, M., W. Wagner, C. Eberhöfer, and W. Karel (2006), Accuracy of large-scale canopy heights derived from LiDAR data under operational constraints in a complex alpine environment, *ISPRS J. Photogramm. Remote Sens.*, *60*, 323–338.
Hubert-Moy, L., A. Cotonnec, L. Le Du, A. Chardin, and P. Perez (2001), A comparison of parametric classification procedures of remotely sensed data applied on different landscape units, *Remote Sens. Environ.*, *75*, 174–187.
Hupp, C. R. (2000), Hydrology, geomorphology and vegetation of Coastal Plain rivers in the south-eastern USA, *Hydrol. Processes*, *14*(16–17), 2991–3010.
Jackson, R. G. (1976), Large-scale ripples of the Lower Wabash River, *Sedimentology*, *23*, 593–623.
Karrenberg, S., J. Kollmann, P. J. Edwards, A. M. Gurnell, and G. E. Petts (2003), Patterns in woody vegetation along the active zone of a near-natural alpine river, *Basic Appl. Ecol.*, *4*, 157–166.
Kasvi, E., M. Vaaja, P. Alho, H. Hyyppä, J. Hyyppä, H. Kaartinen, and A. Kukko (2013), Morphological changes on meander point bars associated with flow structure at different discharges, *Earth Surf. Processes Landforms*, *38*(6), 577–590.
Kleinhans, M. G., and J. H. van den Berg (2011), River channel and bar patterns explained and predicted by an empirical and a physics-based method, *Earth Surf. Processes Landforms*, *36*(6), 721–738.
Kraus, K., and N. Pfeifer (1998), Determination of terrain models in wooded areas with airborne laser scanner data, *J. Photogramm. Remote Sens.*, *53*, 193–203.
Landgrebe, D. A. (2003), Multispectral image data preprocessing, in *Signal Theory Methods in Multispectral Remote Sensing*, John Wiley & Sons, Inc., Hoboken, N. J., doi: 10.1002/0471723800.ch10.
Leeder, M. R., and P. H. Bridges (1975), Flow separation in meander bends, *Nature*, *253*, 338–339, doi:10.1038/253338a0.
Mahoney, J. M., and S. B. Rood (1998), Streamflow requirements for cottonwood seedling recruitment: An integrative model, *Wetlands*, *18*, 634–645.
Marani, M., C. Da Lio, and A. D'Alpaos (2013), Vegetation engineers marsh morphology through multiple competing stable states, *Proc. Natl. Acad. Sci. U. S. A.*, *110*(9), 3259–3263, doi:10.1073/pnas.1218327110.
Mather, P. M., and M. Koch (2011), Classification, in *Computer Processing of Remotely-Sensed Images: An Introduction*, 4th ed., pp. 229–284, John Wiley, Chichester, U. K., doi:10.1002/9780470666517.ch8.
McGowan, J. H., and L. E. Garder (1970), Physiographic features and stratification types of coarse-grained point bars: Modern and ancient examples, *Sedimentology*, *14*, 77–111.
McKenney, R., R. B. Jacobson, and R. C. Wertheimer (1995), Woody vegetation and channel morphogenesis in low-gradient, gravel-bed streams in the Ozark Plateaus, Missouri and Arkansas, *Geomorphology*, *13*, 175–198.
Montserud, R. A., and R. Leamans (1992), Comparing global vegetation maps with the kappa statistic, *Ecol. Modell.*, *62*, 275–293.
Nanson, G. C. (1980), Point bar and floodplain formation of the meandering Beatton River, northeastern British Columbia, *Sedimentology*, *27*, 3–29.
Nanson, G. C. (1981), New evidence of scroll-bar formation on the Beatton River, *Sedimentology*, *28*(6), 889–891.
Nanson, G. C., and H. F. Beach (1977), Forest succession and sedimentation on a meandering-river floodplain, northeast British Columbia, Canada, *J. Biogeogr.*, *4*, 229–251.
Nanson, G. C., and J. C. Croke (1992), A genetic classification of floodplains, *Geomorphology*, *4*(6), 459–486.
Nicholas, A. P. (2013), Modelling the continuum of river channel patterns, *Earth Surf. Processes Landforms*, *38*(10), 1187–1196.
Perucca, E., C. Camporeale, and L. Ridolfi (2006), Influence of river meandering dynamics on riparian vegetation pattern formation, *J. Geophys. Res.*, *111*, G01001, doi:10.1029/2005JG000073.
Perucca, E., C. Camporeale, and L. Ridolfi (2007), Significance of the riparian vegetation dynamics on meandering river morphodynamics, *Water Resour. Res.*, *43*, W03430, doi:10.1029/2006WR005234.
Rozo, M. G., A. C. R. Nogueira, and W. Truckenbrodt (2012), The anastomosing pattern and the extensively distributed scroll bars in the middle Amazon River, *Earth Surf. Processes Landforms*, *37*(14), 1471–1488, doi:10.1002/esp.3249.
Ruiz-Villanueva, V., B. Wyżga, H. Hajdukiewicz, and M. Stoffel (2016), Exploring large wood retention and deposition in contrasting river morphologies linking numerical modelling and field observations, *Earth Surf. Process. Landforms*, *41*, 446–459, doi:10.1002/esp.3832.
Salo, J., R. Kalliola, I. Hakkinen, Y. Makinen, P. Niemela, M. Puhakka, and P. D. Coley (1986), River dynamics and the diversity of Amazon lowland forest, *Nature*, *322*, 254–258.
Seminara, G. (2006), Meanders, *J. Fluid Mech.*, *54*, 271–297.
Solari, L., M. Van Oorschot, B. Belletti, D. Hendriks, M. Rinaldi, and A. Vargas-Luna (2016), Advances on modelling riparian vegetation—Hydromorphology interactions, *River Res. Appl.*, *32*, 164–178, doi:10.1002/rra.2910.
Sundborg, A. (1956), The River Klaralven: A study of fluvial processes, *Geogr. Ann.*, *38*, 127–316.
Surian, N., L. Mao, M. Giacomin, and L. Ziliani (2009), Morphological effects of different channel-forming discharges in a gravel-bed river, *Earth Surf. Processes Landforms*, *34*, 1093–1107, doi:10.1002/esp.1798.

Valente, C. R., E. M. Latrubesse, and L. G. Ferreira (2013), Relationships among vegetation, geomorphology and hydrology in the Bananal Island tropical wetlands, Araguaia River basin, Central Brazil, *J. South Am. Earth Sci.*, *46*, 150–160, doi:10.1016/j.jsames.2012.12.003.

van de Lageweg, W. I., W. M. van Dijk, A. W. Baar, J. Rutten, and M. G. Kleinhans (2015), Bank pull or bar push: What drives scroll-bar formation in meandering rivers?, *J. Sediment. Res.*, *85*, 1238–1257.

van Oorschot, M., M. Kleinhans, G. Geerling, and H. Middelkoop (2016), Distinct patterns of interaction between vegetation and morphodynamics, *Earth Surf. Processes Landforms*, *41*, 791–808.

Wasser, L., R. Day, L. Chasmer, and A. Taylor (2013), Influence of vegetation structure on LiDAR-derived canopy height and fractional cover in forested riparian buffers during leaf-off and leaf-on conditions, *PLoS ONE*, *8*(1), e54776, doi:10.1371/journal.pone.0054776.

Williams, R. D., J. Brasington, D. Vericat, and D. M. Hicks (2014), Hyperscale terrain modelling of braided rivers: Fusing mobile terrestrial laser scanning and optical bathymetric mapping, *Earth Surf. Processes Landforms*, *39*, 167–183, doi:10.1002/esp.3437.

Zen, S., G. Zolezzi, M. Toffolon, and A. M. Gurnell (2016), Biomorphodynamic modelling of inner bank advance in migrating meander bends, *Adv. Water Resour.*, *93*, 166–181, doi:10.1016/j.advwatres.2015.11.017.

Ziliani, L., and N. Surian (2012), Evolutionary trajectory of channel morphology and controlling factors in a large gravel-bed river, *Geomorphology*, *173–174*, 104–117.